Fe Kα Lines of MCG-6-30-15: Emission from Thin-torus Particles around a Kerr Black Hole

J. Z. G. Ma[1*]

[1]*California Institute of Integral Studies, San Francisco, CA, 94103, USA.*

Author's contribution

The sole author designed, analyzed and interpreted and prepared the manuscript.

Original Research Article

We investigate the characteristics of monochromatic particles about a Kerr (rotating) black hole (BH) and their contributions to the observed soft X-ray flux of Fe Kα emission lines. We develop a thin-torus model to formulate the particles which are not restricted within the equatorial plane of the BH, but spherically symmetric and extends to both sides of the equatorial plane due to the gravitational frame-dragging effect. A data-fit modeling to the observed line profile of MCG-6-30-15 indicates that (1) The emission originates from the torus at $13.9 \pm 0.05r_g$ (r_g is the gravitational radius of the BH) with a polar angle of ∼52.2°, instead of from a thin disk in the equatorial plane. (2) In addition to the usually accepted two humps in the observed profile, the blue-shifted one at ∼6.4 keV is caused by prograde particles, and the strongly red-shifted one at ∼4.8 keV by retrograde particles, there exists the third one at ∼5.5 keV. (3) The central BH rotates rapidly with $a = 0.96 \pm 0.005$ (a is the dimensionless specific angular momentum of the BH); (4) Relative to the axis of the BH spin, the inclination angle of observation is 28±0.5°.

Keywords: Physics of black holes; galaxies: individual; line: profiles; X-rays.

Corresponding author: E-mail: zma@mymail.ciis.edu;

1   INTRODUCTION

The nearby Seyfert 1 galaxy MCG-6-30-15 (z=0.008) is one of the best-studied active galaxies in X-ray wavebands[1-5]. In addition to the primary, power-law X-ray continuum which was found in most Seyfert 1 active galactic nuclei (AGNs) (e.g. [6]), the galaxy owns the best-resolved broad but skewed profile of the fluorescent iron Kα lines in the soft X-ray band[7]: on the one side, the profile red-shifts down from the rest-frame energy, 6.35 keV, to $\sim$4.5 keV; on the other side, it blue-shifts up by a little increment of only $\sim$0.2 keV, along with a couple of two peaks at $\sim$5.5 keV and $\sim$6.4 keV in the broader red-wing and the relatively narrower blue-wing, respectively.

At first, the peculiar profile was believed to be driven by both special and general relativistic effects of a Schwarzschild (nonrotating) black hole (BH) on the photons emitted from a standard thin accretion disk outside the BH[7,8]. In such a system, the inner boundary of the disk cannot extend within the radius of the marginally stable orbits, i.e., 6r_g, where $r_g = GM/c^2$ is the gravitational radius of the BH of mass M. Thus, this thin disk model explained that the well-resolved broad Fe Kα line was emitted from the fluorescence of matter in the inner disk less than 20r_g[7,9,10]. In addition, the model claimed that and there were only two humps in the line profile according to the calculated flux based on assuming a double-peak transfer function [see Eq.(1.1) and relevant text in [11] for details].

However, the huge red tail observed in the deep minimum (DM) of the X-ray light curve requires that the line profile should come from a region which is at much smaller radii, e.g., 1.24$\sim$10r_g. In this case, a disk-illumination model of a nonrotating black hole paradigm is unable to predict observed overall profile shapes nor always fit consistently to the disk inclinations[12,13]. Thus, a Kerr (rotating) BH is necessary to drag the disk closer. A comparison with a Schwarzschild case did show that an extreme Kerr BH system is $\sim$3 times more likely to give off the line emission[14] because it appeared unrealistic to bring about the observations of the X-rays from inside of

6r_g, or even closer to the BH horizon, with the thin disk model[15]. Though the consideration might offer an alternative "occultation model" to illustrate the Kerr effects manifested in the DM period, the measured shape of the Fe Kα lines were still regarded as a double Gaussian which did not offer any physical models related to a Kerr BH[16].

Recent observations in MCG-6-30-15 were not in favor of the thin-disk model[17,18]. The new experiments provided consistent results to those predicted by the early theoretical work: BHs are very likely to be rotating and the Kerr metric should be taken into account. The prediction showed that, in the 4D spacetime, bound geodesics of particles in the inner region of the surrounding disk, extending from the hole's horizon at r_g outward to tens of r_g, trace out helix-like spherical orbits by strong gravitational frame-dragging effect between the minimum and maximum latitudes about the equatorial plane of the central hole[19]. This sketch was supported by the observations of a comparable width of the Fe line with the optical ones, indicating a hot torus formed by spherical particles within the inner disk[20].

Therefore, the commonly used thin-disk model with a Schwarzschild-BH model may not still be valid to describe the inner region of the disk outside a central BH (e.g.,[21]). For this reason, this paper proposes an alternative approach to the line emission of MCG-6-30-15 in view of a non-disk thin-torus formulation of monochromatic particles about a Kerr BH. As defined in [15,18], these particles emit identical and isotropic fluorescent Fe Kα lines and occupy all of the possible orbits around the central BH. As a synthesis of previous work on particle's equations[19,22-26] and an extension of previous disk models of line emissions[9,15,17,18], three key parameters, namely, BH angular momentum a, emitter's radial position r, and observer's inclination angle θ, are used to fit the observed profile.

The plan of the paper is as follows: §2 describes the thin-torus formulation of a test particle in a torus in Kerr metric, and shows the criteria of its motion in the stable spherical geodesics bounded outside a Kerr BH; §3 introduces the

relativistic generalization of Liouville's theorem for simulations of the integrated line profiles from monochromatic torus particles; §4 presents results of the simulations and a particular data-fit to the line profile of MCG-6-30-15; finally, conclusions are summarized and discussed in §5.

2 THIN TORUS FORMULATION IN KERR METRIC AND CRITERIA OF MOTION

Choose natural units, $G = c = 1$, and a geometrized radial coordinate r in the unit of $r_g = M$. Parameter r is thus a dimensionless quantity and $r_g = 1$. Fig. 1 depicts the Boyer-Lindquist coordinates in Kerr metric around a BH and the spherical coordinates in the absolute space at infinity. Due to the strong gravitational dragging effect, particles are bounded between the minimum and maximum latitudes in the inner disk about the equatorial plane of the central BH and trace out helix-like spherically symmetric torus orbits[18,21-25]. Torus particles emit Fe K-line photons observed by a distant observer in the image plane of a celestial sphere at infinity who is at rest with respect to coordinates, $t = t_0 = 0$, $r = r_0$, $\theta = \theta_0$, and $\phi = \phi_0 = 0$. the Kerr metric is[22].

$$\left.\begin{aligned}
ds^2 = &-(1 - 2r/\Sigma)dt^2 - \\
&- [4ar(1 - \mu)/\Sigma)]dtd\phi + \\
&+ (\Sigma/\Delta)dr^2 + \Sigma d\theta^2 + \\
&+ [\Lambda(1 - \mu)/\Sigma)]d\phi^2
\end{aligned}\right\} \quad (2.1)$$

where $\Sigma = r^2 + \mu a^2$, $\mu = \cos^2\theta$, $\Delta = r^2 - 2r + a^2$, $\Lambda = (r^2 + a^2)^2 - \Delta(1 - \mu)a^2$; $a = J/M^2$ is the specific reduced magnitude of the angular momentum J of the central BH.

The general trajectories of a test particle, say an iron atom, are described by three constants of motion: E, L_z, and Q. Let m be the rest mass of the test particle, the constants are the energy reduced by m, the angular momentum parallel to symmetry axis reduced by mM, and the Carter's θ parameter reduced by $(mM)^2$, respectively[23].

Four geodesic equations of motion of the particle are as follows[27]:

$$\left.\begin{aligned}
(\Sigma/E)u^t = &-a[a(1 - \mu) - p] + \\
&+ [(r^2 + a^2)/\Delta](r^2 + a^2 - ap) \\
(\Sigma/E)^2(u^r)^2 = R(r) = &-(1/E^2 - 1)r^4 + \\
&+ (2/E^2)r^3 - [a^2(1/E^2 - 1) + \\
&+ (p^2 + q)]r^2 + 2[(a - p)^2 + q]r - a^2q \\
(\Sigma/E)^2(u^\theta)^2 = \Theta(\mu) = \\
= &4\mu\{a^2(1/E^2 - 1)\mu^2 - \\
&- [a^2(1/E^2 - 1) + (p^2 + q)]\mu + q\} \\
(\Sigma/E)u^\phi = &-[a - p/(1 - \mu)] + \\
&+ a/\Delta(r^2 + a^2 - ap)
\end{aligned}\right\} \quad (2.2)$$

where $p = L_z/E$ is the reduced angular momentum in the azimuthal direction and $q = Q/E^2$ is the reduced Carter's constant characterizing the θ motion. $q = 0$ corresponds to the equatorial plane of the BH with $\theta = 90°$.

The requirement of the third equality in Eq. (2.2) restricts $\Theta(\mu) \geq 0$. Thus, $0 \leq \mu \leq \mu_-$, or,

$$90° - \arccos\mu_-^{-1/2} \leq \theta \leq 90° + \arccos\mu_-^{-1/2} \quad (2.3)$$

where $\mu_- = (A - \sqrt{B})/C$ in which $A = a^2(E^{-2} - 1) + (p^2 + q)$, $B = [a^2(E^{-2} - 1) + (p^2 + q)]^2 - 4a^2(E^{-2} - 1)q$, and $C = 2a^2(E^{-2} - 1)$. Eq. (2.3) says that the torus particle is limited in a region symmetrical about the equatorial plane with the maximal polar angle $\arccos\mu_-^{-1/2}$.

Torus particles bounded stable in spherical orbits satisfy following conditions[22,23]: $R(r) = 0$, $dR/dr = 0$, $d^2R/dr^2 = 0$. These equalities give three constants of motion, p, q, and E[27]:

$$\left.\begin{aligned}
p_\pm = &[-B_2 \pm (B_2^2 - 4B_1B_3)^{1/2}]/(2B_1) \\
q = &-\frac{r}{\Delta^2}\{[r(r - 2)^2 - a^2]p^2 + \\
&+ 2a[r(3r - 4) + a^2]p - \\
&- [(r^2 + a^2)^2 - 4a^2r]\} \\
E^2 = &\frac{r^2(r^2 - 2r + a^2)}{r^4 + (a^2 - p^2 - q)r^2 + 2[(a - p)^2 + q]r - a^2q}
\end{aligned}\right\} \quad (2.4)$$

where the sign "±" gives the the limits of p, and, $B_1 = A_2/A_1 - A_5$, $B_2 = A_3/A_1 - A_6$, $B_3 = -A_4/A_1 + A_7$; $A_1 = 5r^4 - 16r^3 + 6(a^2 + 2)r^2 - 8a^2r + a^4$, $A_2 = \Delta^2(5r^3 - 16r^2 + 12r - 2a^2)$, $A_3 = 4a\Delta^2(6r^2 - 6r + a^2)$, $A_4 = 2\Delta^2(3r^4 + 4a^2r^2 - 6a^2r + a^4)$, $A_5 = r(r - 2)^2 - a^2$, $A_6 = 2a[r(3r - 4) + a^2]$, $A_7 = (r^2 + a^2)^2 - 4a^2r$.
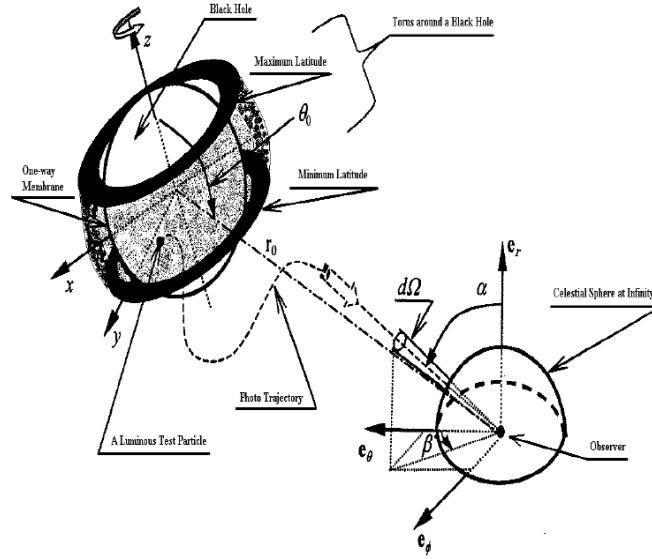
Fig. 1. Coordinates and diagram of the luminous torus in Kerr metric. Torus particles emit Fe Kα photons observed by a distant observer in the image plane of a celestial sphere at infinity who is at rest with respect to Boyer-Lindquist coordinates, $t = t_0 = 0$**,** $r = r_0$**,** $\theta = \theta_0$**, and** $\phi = \phi_0 = 0$

Eq. (2.4) indicates that the three constants have their defined regions one each, and change differently with the increase of r. For any values of a, E is always larger than zero and levels off to 1. q is never lower than zero. That is to say, besides the equatorial plane ($q = 0$), there are also abundant non-disk orbits for $q \neq 0$. The values of p has two sets, one is positive and the other is negative, indicating that a particle is either co-revolving or counter-revolving relative to the BH spin[19].

3 IRON Kα LINE EMISSION FROM MONOCHROMATIC PARTICLES IN THE TORUS

Based on previous studies, e.g., [15,18], we assume an isotropic line emission and the emitted fluorescent Fe Kα line from particles is described by a δ-function in frequency, giving each emitted photon an energy of 6.35 keV. That is, particles are supposed monochromatic in radiations. Besides, luminous particles are assumed to occupy all of the possible orbits defined by the three constants of motion.

The relativistic generalization of Liouville's equation[28-30] expresses that the observed spectral flux density, F_{line}, follows[9,18,31-36]

$$
\left. \begin{array}{l} F_{line}(\nu, \ r_0, \ \theta_0, \ r, \ a) = \\ = \sum_q \int d\nu d\Omega \cdot I \ \cdot (\frac{\nu}{\nu_E})^3 \cdot \cos\alpha \end{array} \right\} \quad (3.1)
$$

where ν is the observed frequency in the local image plane of a distant observer at $\{r_0, \ \theta_0, \ \phi_0\}$; $\nu_E = 6.35\text{keV}/h$ where h is the Planck constant; $d\Omega$ is the element of the solid angle which covers the image of the spherical ring in the observer's sky with the polar angle α. Considering the symmetric metric about the BH axis, take $\phi_0 = 0$. The ratio of ν/ν_E is the general relativistic frequency shift, and $(\nu/\nu_E)^3$ arises because along the entire trajectory of the photon, $I/\nu^3 = I_e/\nu_E^3$ is an invariant resulting from the conservation of photons in a flux tube together with conservation of volume in phase space. The sum $\sum$ is to all values of q, which reflects the flux is a superposition of images formed by sets of trajectories of the photon emitted from emitters to the observer's sky.

In Eq. (3.1), $I = (1/2) \times 2hN\nu_E^3$ is the specific intensity of photons with the unit of ergs s^{-1} cm^{-2} sr^{-1} eV^{-1}. In this formula, coefficients

$1/2$ and 2 mean that there are only half of photons emitted outwards and there exists two states of the photon quantum per phase-space, respectively. In addition, N (cm^{-3} dyn^{-3} s^{-3}) is the photon distribution function:

$$N(x^\mu, u^\mu, s^\mu) = C(x^\mu) \cdot \delta(u^\mu s_\mu - h\nu_E) \quad (3.2)$$

where $x^\mu = \{t, r, \theta, \phi\}$; $u^\mu = \{u^t, u^r, u^\theta, u^\phi\}$ as shown in Eq. (2); $C(x^\mu)$ (cm^{-3}) is photon's number density (let $C = 1$ hereafter, that is, not considering the inhomogeneity of photons); s^μ is photon's 4-momentum with three covariant Boyer-Lindquist components, s_t, s_θ, and s_ϕ[24]:

$$\left. \begin{array}{l} s_t = -h\nu, \\ s_\theta^2 = \frac{(Mh\nu)^2[\Sigma\Lambda + 4ar\Sigma x - (\Sigma - 2r)x^2/(1-\mu)]}{\Lambda(1 - 2r/\Sigma) + 4(ar)^2(1-\mu)/\Sigma}, \\ s_\phi = Mh\nu\rho\cos\beta\sin\theta\sin\theta_0 \end{array} \right\}$$

(3.3)

where $\rho = r\sin\alpha$ is photon's impact parameter, $x = \rho\cos\beta\sin\theta_0$; β is the azimuthal angle in the image plane at infinity.

Liouville's theorem expressed by Eq.(3.1,3.2) shows that the line emission of the luminous particles is dependent of not only the four-velocity & four-coordinate components but also the invariant four-momentum of photons. This demonstrates that both the null geodesics of photons and the trajectories of emitters are responsible for the emission of the observed line flux.

With more details in mathematics, a tedious algebra gives the measured dimensionless relative flux F[36]. It depends on the three parameters: the BH spin a, the radial position r of the torus emitters, and the inclination angle θ_0 of the observer, as expressed by

$$F = \frac{r_0^2}{h\nu_e} F_{line} = C_1 \cdot \sum_q \int (C_2 + C_3)\cos\alpha \quad (3.4)$$

where

$$\left. \begin{array}{l} C_1 = \frac{\nu/\nu_e}{2\cdot\sin^2\theta_0\cdot E\cdot T_{13}} \\ C_2 = \frac{dW^2}{T_{19}\cdot\sqrt{W^2 - [T_{17} + a(1-\mu)]^2}} \\ C_3 = \frac{dW^2}{T_{20}\cdot\sqrt{W^2 - [T_{18} + a(1-\mu)]^2}} \end{array} \right\}$$

(3.5)

in which

$$\left. \begin{array}{l} T_{20} = 1 - (T_{14} - 1) \cdot T_{18}/C_4 \\ T_{19} = 1 - (T_{14} - 1) \cdot T_{17}/C_5 \\ T_{18} = (-T_{15} - \sqrt{T_{15}^2 - T_{14} \cdot T_{16}})/T_{14} \\ T_{17} = (-T_{15} + \sqrt{T_{15}^2 - T_{14} \cdot T_{16}})/T_{14} \\ T_{16} = T_{15}^2 - T_{10} \cdot (T_{14} - 1)(1 - \mu) \\ T_{15} = -T_{11}/T_{13} - E_e/E^2/T_{13} + a(1-\mu) \\ T_{14} = 1 + \frac{1}{1-\mu}\left(\frac{T_{12}}{T_{13}}\right)^2 \\ T_{13} = u^\phi, \\ T_{12} = u^\theta, \\ T_{11} = u^t \\ T_{10} = \sqrt{W}/\sin\theta_0 \\ T_9 = q \\ T_8 = p \\ T_7 = \Lambda \\ T_6 = \Sigma \\ T_5 = \Delta \\ T_4 = \coth\theta_0 \\ \alpha = -s_\phi/\sin\theta_0 \\ \beta = \sqrt{s_\theta^2 + a^2(1 - \sin\theta_0^2) - s_\phi^2 \cdot T_4^2} \\ C_4 = \sqrt{T_{15}^2 - T_{16} - (T_{14} - 1) \cdot T_{18}^2} \\ C_5 = \sqrt{T_{15}^2 - T_{16} - (T_{14} - 1) \cdot T_{17}^2} \end{array} \right\}$$

(3.6)

4 PROFILES OF IRON Kα LINE EMISSION

As obtained in the last Section, Eq.(3.4) gives the formula to calculate the profiles of the iron Kα line emissions. Numerical calculations cover a wide range of the three parameters: $\{r, a, \theta_0\} = \{0\sim40, 0\sim0.999, 0\sim90°\}$ with steps of $\{0.1, 0.01, 1°\}$. For the data-fit modeling, because the maximal energy resolution in the observation of MCG-6-30-15 [7] is seven sampled points in each spectrum unit 1 keV, corresponding to the sampling step of 0.143 keV, we first try 0.05 and 0.1 keV as the numerical step, respectively, which are higher than the measurement resolution. The obtained profiles are superimposed upon each other in the two cases, except more peaks to be produced in the former case. We thus select 0.1 keV. With the progress of every step, F changes continuously and, only in the regions of $\{r, a, \theta_0\} = \{3\sim15, 0.70\sim0.999, 10\sim45°\}$ can simulations show comparable features of double peaks, skewed line profiles to the observed ones of the Seyfert 1 galaxies.

However, there exists the prescribed minima of a for any set of $\{r, \theta_0\}$, below which there are no data calculated. Besides, F is very sensitive to the three parameters. For a different set of $\{r, a, \theta_0\}$, there always occurs a different profile if carefully examined. That is, there is a relationship of one-to-one correspondence between a profile and a set of the three parameters. The examples of these results are shown in Fig. 2 and Fig. 3, in which all the panels are drawn from part of data calculated with hundreds of sets of three parameters.

4.1 Line Profiles as a Function of the BH Spin

Fig. 2 presents variations of F versus ν/ν_E under different a conditions with $r = 4$ and $\theta_0 = 29°$. Increases in a bring about variations in F from (a) to (i): At first, there is no line emission; Gradually, the flux width extends from the redshift side with one hump to the blueshift side with double or three humps at last. For other values of r and θ_0, there exist similar tendencies.

The results validate Wilkins's theory[18]: For a definite value of a, stable spherical particles can only exist outside the minimal radius, r_{min}; For a definite value of r, stable spherical particles can only exist beyond the minimal spin, a_{min}. For $r = 4$ and $\theta_0 = 29°$, there are no data calculated if $a_{min} = 0.56$. That is, there are no flux from stable torus particles when the spin of the BH is lower than 0.56, needless to say the Schwarzschild case of $a = 0$. In other words, if we detect any flux, the BH spin, a, cannot be less than 0.55 for $r = 4$ and $\theta_0 = 29°$. Thus, without loss of generality, we argue that models of a Schwarzschild BH system may seem too difficult to describe the observed Fe K-line profiles.

4.2 One-to-one Correspondence of Line Profiles with Sets of Three Parameters

Fig. 3 gives nine panels to show how sensitive the profiles are in response to the emitter's radial position, the BH spin, and the observer's inclination angle. The parameter set of the central panel (e) is $\{r = 13.9, a = 0.96, \theta_0 = 28°\}$. In $\nu/\nu_E \sim 0.7 - 1.2$, there are three humps peaking at ~ 0.76, ~ 0.87, and ~ 1.04, respectively.
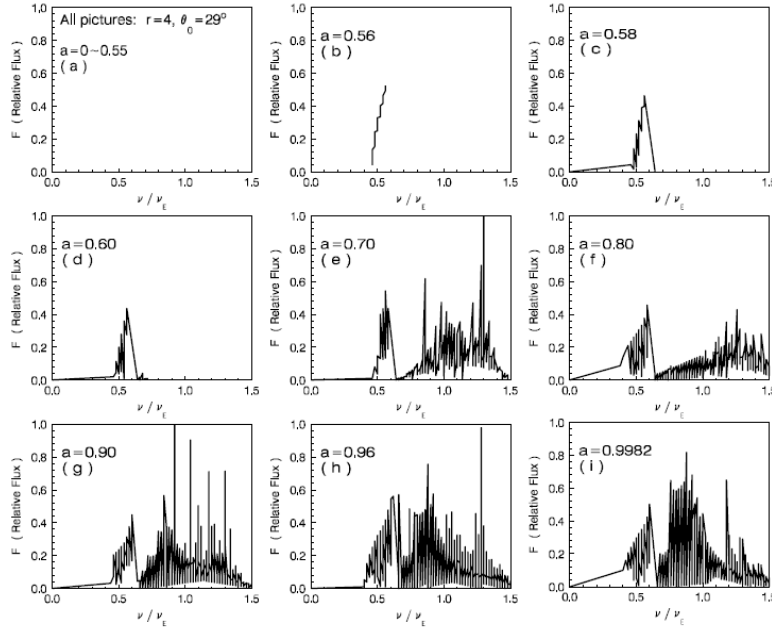
Fig. 2. Normalized dimensionless flux of Fe Kα line, $F = [r_0^2/(h\nu_E)]F_{line}$, as a function of the general relativistic frequency shift, ν/ν_E, in cases of different a from (a) to (i) with $r = 4$ and $\theta_0 = 29°$
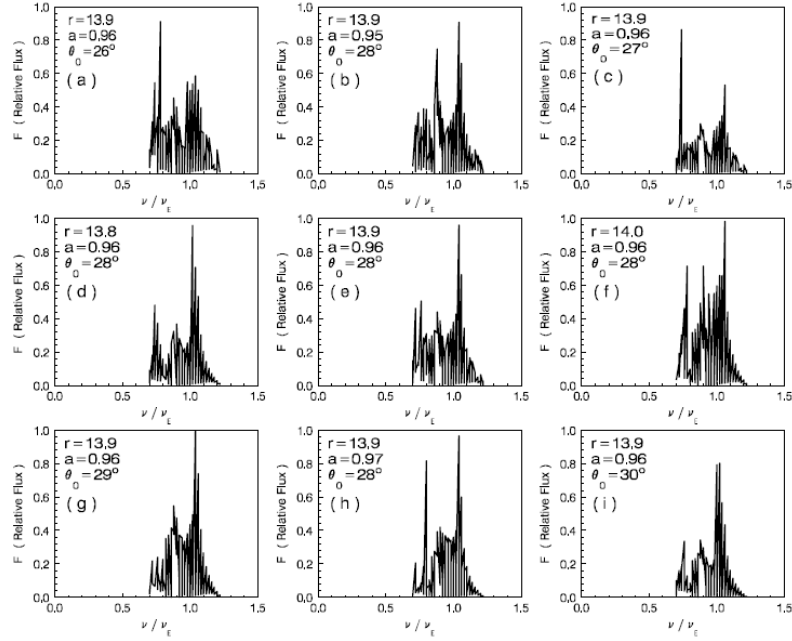
Fig. 3. Normalized dimensionless flux of Fe Kα line, $F = [r_0^2/(h\nu_E)]F_{line}$, as a function of the general relativistic frequency shift, ν/ν_E, with different sets of three parameters: $\{r, a, \theta_0\}$(see text for details). Three panels (d), (e), (f), in the middle row are the cases of r=13.8, 13.9, and 14.0 while other two parameters are not changing. Three panels (b), (e), (h), in the middle column correspond to a=0.95, 0.96, and 0.97, respectively, with other two parameters constant. Five panels (a), (c), (e), (g), (i), give the cases that θ_0 is changing between $26°$ and $30°$ while other two parameters are stable

Three ones in the middle row, (d), (e), and (f), is the case when r is changing in steps with other two parameters of $a = 0.96$ and $\theta_0 = 28°$. One obvious difference lies in the relative heights of three peaks for different r. Another distinction is in the changes of troughs at both $\sim$0.80 and $\sim$0.95. However, there are no regularities in above variations. We note that the radial positions of all peaks and troughs seems stable in the three panels.

The other three panels in the middle column, (b), (e), and (h), and the other five ones, (a), (c), (e), (g), (i), are those under conditions of different a while r=13.9 and $\theta_0 = 28°$ and a changing θ_0 with r=13.9 and a=0.96, respectively. They illustrate similar results that the relative strengths of three humps, as well as the patterns of troughs, are present in each set of the three parameters.

Of all the panels drawn, we conclude that every set of the three parameters offers a specific profile which is unable to be produced by any other sets of the three parameters. That is to say, although there is no accurate rules of the profile variations with different sets of parameters, there exists an one-to-one correspondence between one profile and one set of the three parameters. It is just this kind of relation that make it possible for us to determine the physical features of different Seyfert or Seyfert-like galaxies from the observed Fe Kα lines.

4.3 Data-Fit to the Fe Kα Line Profile of MCG-6-30-15

Previous studies [9,14,17] predicted that the observed Fe Kα line shape in MCG-6-30-15[7] corresponds to a BH-disk system with a high spin close to the extreme angular momentum and an inclination angle around $30°$. We present

here the data-fit simulations with our thin-torus formulation. The result, Fig. 3(e), is given in the top panel of Fig. 4 below, where the abscissas are selected in units of keV. In this figure, our data-fitting result is compared with that observed by Tanaka et al [7] where the authors suggested an accretion disk to exist in MCG-6-30-15. The observed profile is redrawn in the bottom panel which occurred as Fig. 2 in Tanaka et al's paper.

Fig. 3(e) is the best-fitting one to Fig. 2 of [7] in the Fe Kα line region of 4.5–7.2 keV. As mentioned above, the sampling step of the observation was 0.143 keV. We thus rebin the numerical step as 6.35/50 keV=0.127 keV, which is close to but a little higher than the instrumental resolution for realistic data-fit simulations. Calculations with the rebinned step are shown in Fig. 4.
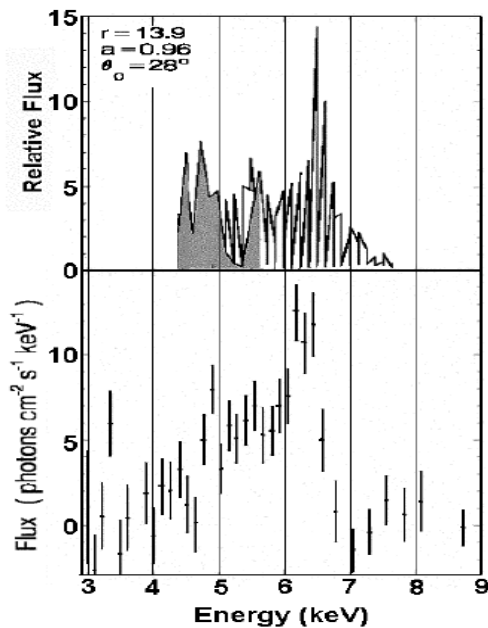
Fig. 4. Line profiles of both the data-fitting profile and the observed profile. The former is Fig. 3(e) shown in the top panel; the latter is from [7] shown in the bottom panel. The abscissas are in units of keV

Profiles in the two panels of Fig. 4 demonstrate following similarities:

(1) Both of them have three humps from 4.5 keV to 7.2 keV at $\sim$4.8 keV, $\sim$5.5 keV and $\sim$6.2–6.6 keV, respectively. The middle hump has the lowest intensity and the right one has the highest intensity.

(2) Both of them are significantly asymmetric about the line emission energy, $E_e = 6.35$ keV, with a much more extended red wing (i.e., red-shifted hump) on the left-hand-side profile than a narrow blue wing (i.e., blue-shifted hump) on the right-hand side.

(3) Both the red-shifted hump and the blue-shifted hump drop sharply at $\sim$4.6 keV and $\sim$6.7 keV, respectively. Between them, there appears the third hump. This three-hump identification is different from the previous argument that there exist merely two peaks[7,10].

The data-fit modeling with our thin-torus formulation suggests a Kerr BH system in MCG-6-30-15: Firstly, the central BH in the galaxy is rotating with $a = 0.96 \pm 0.005$, very close to the maximal spin $a = 0.9982$ of a Kerr BH[37]. This result is in accordance with those of [9,10,13,14]. Secondly, the position of the emission line is at $13.9 \pm 0.05 r_g$, which means that the line emission does not come from a region very close to the BH. We note that Ref.[11] showed that the outer radius is $13.3 r_g$ in Table 1 of the paper for the Kerr model. We argue that it is the particles of the torus with a radius of $13.9 r_g$, rather than those of the thin disk in the equatorial plane, that emit the observed flux. From Eqs. (2.3) and (2.4), this thin torus extends to $\pm \sim 52.2°$ from the equatorial plane. At last, the inclination angle is $28 \pm 0.5°$, which is in good agreement with the results either using a nonrotating BH model[8] or a Kerr BH one[16], in which the angles are usually predicted around $30°$.

The upper panel of Figure 4 also reveals line emissions from both prograde and retrograde particles. The unshadowed profile is produced by the former while the shadowed one by the latter. It is clear that the prograde particles contribute the intense blue hump at $\sim$6.5 keV, while the retrograde ones do the deeper redshifted hump at $\sim$4.8 keV; both kinds of particles jointly produce the redshifted hump between these two humps.

5 CONCLUSION

This paper extends a commonly accepted thin disk model to a thin torus model under following considerations: (1) Particles in the inner disk are in fact existed in the spherical torus between the minimum and maximum latitudes about the equatorial plane of the central BH; (2) the thin disk model assumed a double-peak transfer function which was an over-simplified description for the observed broad Fe $K\alpha$ line emissions.

We simulate the Fe line profiles under different set of the three parameters (BH spin, emitter's radius, and observer's inclination angle). We find an one-to-one correspondence between sets of and the Fe $K\alpha$ line profiles. This is important in following studies to apply our thin torus model in identifying the physical properties of BH systems existing in astronomical objects observed with Fe $K\alpha$ line emissions. Specifically for MCG-6-30-15, we conclude that:

(1) The central BH is rapidly spinning with $a = 0.96 \pm 0.005$, resulting in a thin torus of luminous particles which extends to both sides of the equatorial plane with a polar angle of $\sim 52.2°$, rather than residing in the disk on the equatorial plane.

(2) The torus particles have two types: co-revolving or prograde ($p > 0$) and counter-revolving or retrograde ($p < 0$) [see the expression of p in Eq. (2.4)]. They produce two wings of the line emission in the observer's sky: the former type contributes to the blue-shifted wing with one hump at ~ 6.4 keV; the latter one causes the red-shifted wing with another hump at ~ 4.8 keV.

(3) Between the two humps, there is the third hump at ~ 5.5 keV. Though it was observed, as shown in the bottom panel of Figure 4[7], it was usually neglected in the disk model. In view of our thin torus model, this hump is a hybrid contribution of the two groups of particles relative to the observer's sky: approaching particles among the retrograde ones and the receding particles among the prograde ones.

(4) The emission originates from the torus at $13.9 \pm 0.05 r_g$, and is observed at infinity with an inclination angle of observation $28 \pm 0.5°$, relative to the axis of the BH spin.

We suggest that there exist three broadening factors which contribute to the widths of the observed three humps: (1) Gravitational or general relativistic shift α_1; (2) Transverse or special relativistic Doppler shift α_2; and (3) Classical or longitudinal Doppler shift α_3. α_1 is named as lapse function and is the ratio of the lapse of proper time to that of global time[38]. It leads only to the red-shifts of a line emission. Different from α_1, α_2 and α_3 can bring about both blue-shifts and red-shifts of line emission.

In dealing with more Seyfert(-like) galaxies, however, we mention here that, although the basic physics could be the same as discussed in this paper, the relative strengths of humps and the patterns of troughs in observed profiles may be different. This is because the relatively blue-shifted wing might not be necessarily extending to the blue-shifted band relative to the rest-energy of the emission line. Our simulations revealed that the blue-shifted wing is really in the red-shifted band with some sets of three parameters, while the red-shifted wing extends further to the lower energy band. In this case, there is no hump at the frequency higher than the rest-frequency.

It deserves to note that, although the disk model still prevails the data-fit modeling to investigate the broad Fe line emissions from active galactic nuclei ([39] and references therein), recent studies presented the possibility to use the lines to estimate the parameters of central supermassive black holes and the properties of the BLR gas near the black holes, not only their masses, but also their spins ([40] and references therein). As a companion work with the most recent study on the broad iron $K\alpha$ emissions from NGC 3516[36], this paper chose the famous source, MCG-6-30-15, to confirm that the non-disk torus model for a Kerr black-hole system provides an alternative explanation on the particle dynamics, black-hole spinning states, and line emission mechanism. The two studies mutually support that it is a rotating black hole system with a luminous torus (not a disk) that exists in Fe-line-emission objects.

COMPETING INTERESTS

Author has declared that no competing interests exist.

References

[1] Nandra K, Pounds KA, Stewart GC. The X-ray spectrum of MCG-6-30-15 and its temporal variability. MNRAS 1991;242:660-668.

[2] Nandra K, Pounds KA. GINGA observations of the X-Ray spectra of Seyfert galaxies. MNRAS. 1994;268:405-429.

[3] Fabian AC, Kunieda H, Inoue S, et al. ASCA observations of the warm absorber in MCG-6-30-15: The discovery of a change in column density. PASJ. 1994;46:L59-63.

[4] Tanaka Y, Inoue H, Holt SS. The X-ray astronomy satellite ASCA. PASJ. 1994;46:L37-41.

[5] Reynolds CS, Fabian AC, Nandra K, et al. ASCA PV observations of the Seyfert 1 galaxy MCG-6-30-15: rapid variability of the warm absorber. MNRAS. 1995;277:901-912.

[6] Nandra K, George IM, Mushotzky RF, et al. ASCA observations of Seyfert 1 galaxies. I. Data analysis, imaging, and timing. ApJ. 1997;476:70-82.

[7] Tanaka Y, Nandra K, Fabian AC, et al. Gravitationally redshifted emission implying an accretion disk and massive black hole in the active galaxy MCG-6-30-15. Nature. 1995;375:659-661.

[8] Fabian AC, Rees MJ, Stella L, White NE. X-ray fluorescence from the inner disc in Cygnus X-1. MNRAS. 1989;238:729-736.

[9] Bromley BC, Chen K, Miller WA. Line emission from an accretion disk around a rotating black hole: Toward a measurement of frame dragging. ApJ. 1997;475:57-64.

[10] Weaver KA, Yaqoob T. On the evidence for extreme gravity effects in MCG-6-30-15. ApJ. 1998;502:L139-142.

[11] Laor A. Line profiles from a disk around a rotating black hole. ApJ. 1991;376:90-94.

[12] Sulentic JW, Marziani P, Calvani M. Disk models for MGC -06-30-15: The variability challenge. ApJ. 1998;497:L65-L68.

[13] Sulentic JW, Marziani P, Zwitter T, et al. On the origin of broad Fe Kα and H I Hα lines in active galactic nuclei. ApJ. 1998;501:54-68.

[14] Dabrowski Y, Fabian AC, Iwasawa K, et al. The profile and equivalent width of the X-ray iron emission line from a disc around a Kerr black hole. MNRAS. 1997;288:L11-15.

[15] Branduardi-Raymont G, Sako M, Kahn SM, et al. Soft X-ray emission lines from a relativistic accretion disk in MCG -6-30-15 and Mrk 766. A&A. 2001;365:L140-145.

[16] Cunningham CT. The effects of redshifts and focusing on the spectrum of an accretion disk around a Kerr black hole. ApJ. 1975;202:788-802.

[17] Iwasawa K, Fabian AC, Reynolds CS, et al. The variable iron K emission line in MCG-6-30-15. MNRAS. 1996;282:1038-1048.

[18] Wilkins DC. Bound Geodesics in the Kerr Metric. Phy. Rev. D. 1972;5:814-822.

[19] Chen K, Halpern JP. Structure of line-emitting accretion disks in active galactic nuclei - ARP 102B. ApJ. 1989;344:115-124.

[20] Collin-Souffrin S, Dumont AM. Line and continuum emission from the outer regions of accretion discs in active galactic nuclei. II. Radial structure of the disc. A&A. 1990;229:292-301.

[21] Carter B. Global structure of the Kerr family of gravitational fields. Phys. Rev. 1968;174:1559-1571.

[22] Bardeen M, Press W, Teukolsky S. Rotating black holes: Locally nonrotating frames, energy extraction, and scalar synchrotron radiation. ApJ. 1972;178:347-370.

[23] Stewart J, Walker M. Black holes: The outside story. Springer Tracts in Modern Physics. 1973;69:69-115.

[24] Karas V, Vokrouhlicky D, Polnarev AG. In the vicinity of a rotating black hole - A fast numerical code for computing observational effects. MNRAS. 1992;259:569-575.

[25] Zakharov AF. On the hotspot near a Kerr black hole: Monte-Carlo simulations. MNRAS. 1994;269:283-288.

[26] Chandrasekhar S. The mathematical theory of black holes. New York: Oxford University Press. 1983;363.

[27] Ma ZG. Geodesics of bounded particles around a Kerr black hole. Ch A&A. 2000;24:135-144.

[28] Thorne KS. Relativisitc stellar structure and dynamics. In: Dewitt C, Schatzman E, Veron P, eds. High Energy Astrophysics. New York: Science Publishers, 1967; 3:259-441.

[29] Ames WL, Thorne KS. The optical appearance of a star which is collapsing through its gravitational radius. ApJ. 1968;151:659-670.

[30] Gerlach UH. Optical appearance of a collisionless gas of stars surrounding a black hole. ApJ. 1971;168:481-493.

[31] Hollywood JM, Melia F. General relativistic effects on the infrared spectrum of thin accretion disks in active galactic nuclei: Application to Sagittarius A*. ApJS. 1997;112:423-455.

[32] Ma ZG. Frame-dragging effect of a luminous ring in the generalized orbits around a black hole. Acta Astron. Sin. 2000;41:153-162.

[33] Ma ZG. Iron Kα emission lines in Seyfert(-like) active galactic nuclei: Revelation of a rapidly spinning central black hole. Ch Phys Lett. 2002;19:1527-1539.

[34] Ma ZG. Fe Kα lines of Seyfert I galaxies: Thin-torus model. In: Li XD, Trimble V, Wang ZR, eds. High Energy Processes and Phenomena in Astrophysics. IAU Symposium. San Francisco: Astronomical Society of the Pacific, 2003;214:275-280.

[35] Zakharov AF, Ma ZG, Bao Y. The iron Kα lines as a tool for magnetic field estimations in non-flat accretion flows. New Astron. 2004;9:663-677.

[36] Ma JZG. Broad iron Kα emissions from NGC 3516: Revelation of a non-disk torus around a Kerr black hole with a detailed formulation on the emission mechanism. J Phys Astron. 2016;4:1-16.

[37] Thorne KS. Disk-accretion onto a black hole. II. Evolution of the hole. ApJ. 1974;191:507-520.

[38] Macdonald D, Thorne KS. Black-hole electrodynamics - an absolute-space/universal-time formulation. MNRAS. 1982;198:345-382.

[39] Fabian AC, Iwasawa K, Reynolds CS, Young AJ. Broad Iron Lines in Active Galactic Nuclei. PASP. 2000;112:1145-1161.

[40] Ilić D, Popović LČ. Supermassive black holes and spectral emission lines. J. Phys. 2014;548:012002(1-7).

Peer-review history:
The peer review history for this paper can be accessed here:
http://sciencedomain.org/review-history/17134